Anapole-Assisted Low-Power Optical Trapping

By

Yuxi Jiang

Thesis

Submitted to the Faculty of the

Graduate School of Vanderbilt University

in partial fulfillment of the requirements

for the degree of

MASTER OF SCIENCE

in

Electrical Engineering

May 31, 2021

Nashville, Tennessee

Approved:
Justus C. Ndukaife, Ph.D.
Sharon M. Weiss, Ph.D.

TABLE OF CONTENTS

Page

LIST OF FIGURES

Figure **Page**

Chapter I. Introduction

1. Optical trapping

Optical trapping and related particles manipulation are developing tools in micro and nano scale technology since the observation of optical scattering and gradient forces was first reported in 1970[1]. In the past decades, researchers have successfully achieved the particles trapping in micrometer scale and subnanometer scale[2–4]. In nanometer scale, however, it is necessary to implement nanostructures to complete the optical trapping by generating strong light intensity hotspot in nanoscale volume. People have proposed numerous nanostructures such as plasmon-enhanced nanoantennas, nanoholes to build up the plasmonic nanotweezers platform[5–9]. However, because of the intrinsic lossy nature of the plasmonic material, the absorption of light upon resonant excitation causes significant heat generation that limits the applications for plasmon-assisted optical trapping of biological specimens[10]. Thus, it is important to avoid the heating effect with using a low loss nanotweezer platform. On the other hand, a desired optical nanotweezer platform should possess the capability to simultaneously perform enhanced nano-optical trapping as well as to rapidly transport target objects to the illuminated nanoantenna, while ensuring the objects are trapped at a region of minimal temperature rise. Taking these factors into consideration, in this thesis, a dielectric-metal hybrid nanoantenna system was established to provide an enhanced electromagnetic hotspot in the dielectric region that is spatially dislocated from the thermal hotspot in the metal region. The electromagnetic field in the dielectric region is highly enhanced and therefore can be used to generate a strong optical trapping force as well as tight trapping potential, while the thermal hotspot in the metal region provides the means to initiate rapid electrothermoplasmonic flow on-demand to the trapping site, mitigating the need to rely on Brownian diffusion. In this section, the optical trapping basic function will be introduced.

In this section, the basic principle of the optical trapping will be introduced. In the simplest condition of the optical response on a nanostructure, a dipole approximation can usually be applied to explain the optical force that exerted on a Rayleigh scatterer[11]. The polarizability was determined by

$$\alpha = \frac{\alpha_0}{1 - \frac{ik^3\alpha_0}{6\pi\varepsilon_0}},$$

where α_0 is given by the Clausius-Mossotti relation denoted the point like particle polarizability. Here the time-averaged force of the term that related to intensity gradient can be written as[12]

$$F_{grad} = \frac{1}{4}\mathrm{Re}(\alpha)\nabla|E|^2,$$

which is related to the light intensity gradient field. As the function shown above, the gradient force is related to the light intensity where α is the polarizability of the Rayleigh scatterer. On the other hand, the scattering force of the second term is generated because of the radiation pressure along the light propagation direction as shown below[12]

$$F_{scat} = \frac{\sigma}{2c}\mathrm{Re}(E \times H^*).$$

By using the nano structures people can get the localized hotspot within nano size volume, with thousands of times light intensity enhancement. Therefore, in nanoscale structure the gradient force dominates since the

appearance of high light intensity hotspots. The way that people used to trap nano scale objects are called optical nanotweezers.

Beyond the dipole approximation on the other hand, the numerical calculation on arbitrary particles, such as nanowires, can be done by using Maxwell stress tensor (MST) method

$$\vec{\mathbf{F}} = \oiint \vec{\vec{\mathbf{T}}} \cdot \mathrm{d}\vec{\mathbf{A}},$$

where $\vec{\vec{T}}$ is the Stress tensor that accounting for the interaction between electromagnetic forces and mechanical momentum that got from scattered electromagnetic field as following

$$\mathrm{T_{ij}} = \varepsilon_0 \left(\mathrm{E_i E_j} - \frac{1}{2}\delta_{\mathrm{ij}} \mathrm{E}^2 + \frac{1}{\mu_0}\left(\mathrm{B_i B_j} - \frac{1}{2}\delta_{\mathrm{ij}} \mathrm{B}^2 \right) \right).$$

With using the MST method, people can calculate the optical force exerted on arbitrary closed surface. In the numerical calculation process, as far as the results of the electromagnetic field has been solved, i.e. electric field and magnetic field, the optical force can be derived based on the above equations. Also, by integrating the force along the particles moving direction, the trapping potential can be calculated with the unit of K_BT that shows the capability to overcome the intrinsic Brownian motion and outside disturbing.

2. Optical Anapole Mode

Generating high electromagnetic field enhancements in nanoscale volumes is important to enhance light-matter interaction for myriads of applications in bio-sensing, optical switching and information processing, and optical nanotweezing[13–16]. Within the past decades, plasmonic nanostructures have been actively investigated as a powerful approach to achieve highly enhanced electric field intensities and to confine the light fields into extremely small sub-wavelength volumes[17,18] owing to the excitation of surface plasmon waves. However, because of the intrinsic lossy nature of the plasmonic material, the absorption of light upon resonant excitation causes significant heat generation that limits the applications for plasmon-assisted optical trapping of biological specimens[10]. To mitigate the challenge of heat dissipation encountered with plasmonic systems, high refractive index dielectric materials have generated significant interest as a means to achieve enhanced electromagnetic field intensities and light confinement without an accompanying loss-induced heating effect.

In this section we discuss the anapole mode inside the dielectric nanostructure. Anapole was first been proposed in theoretical physics and was recently used to illustrate a classical model of dark matter[19]. In the simplest cases the anapole mode can be illustrated by the superposition and destructive interference of electric dipole and toroidal dipole, where they can cancel each other in far-field scattering at the resonance wavelength[20]. Thus, when the anapole mode is excited, the light energy is highly confined with an increased electromagnetic field enhancement. The anapole mode has been explored in several antenna geometries including nano-spheres[21] and nano-disks[20,22], which are more amenable for lithographic fabrication. In the single silicon disk, several anapole mode orders could be generated if the disk size is large enough[23]. Different anapole modes can be attributed to the hybrid Mie-Fabry-Perot[24] resonance or the superposition of internal modes contributions[25].

Preliminary research findings have suggested that dielectric nano-disk design could be used to boost the performance of nanophotonic devices for bio-sensing[26] and third-harmonic generation[27,28].

3. Electro-thermo-plasmonic Flow

The optical resonance of nanostructures can support localized tightly optical trapping on nanoscale objects. An issue has raised subsequently that how to transport the objects towards the light intensity hotspot in a microscale environment. In the conventional nanotweezer, people mostly relay on the Brownian motion of objects, which is a slow process that limits the experiments and applications. A long-range fluid condition has been introduced to achieve the fast transport of particles, which is call Electro-thermo-plasmonic (ETP) effect. By taking the advantage of the plasma induced heating effect of nanostructures with using the alternating current (AC) electric field, a vertax fluid condition can be generated[9,29,30]. The ETP flow can be used to induce long-range transport towards the trapping site.

We consider the means of harnessing a spatially dislocated thermal hotspot for induced a long-range ETP flow and thermophoretic force that will aid in particle transport and improved stability. The body force per unit volume in the fluid for the ETP is given by[31]

$$\mathrm{F_{ETP}}(\mathbf{r}) = \frac{1}{2}\mathrm{Re}\left[\frac{\varepsilon(\alpha-\beta)}{1+i\omega\tau}(\nabla \mathrm{T}(\mathbf{r})\cdot\mathbf{E_{ac}})\mathbf{E_{ac}^{*}} - \frac{1}{2}\varepsilon\alpha|\mathbf{E}_{\boldsymbol{ac}}|^{2}\nabla \mathrm{T}(\mathbf{r})\right]$$

, where in the function $\alpha = (1/\varepsilon)(\partial\varepsilon/\partial \mathrm{T})$ and $\beta = (1/\sigma)(\partial\sigma/\partial \mathrm{T})$, σ and ε are conductivity and permittivity of the fluid at the angular frequency ω of the applied electric field. $\tau = \varepsilon/\sigma$ is the charge relaxation time of the fluid. This body force term serves as the forcing term in the Navier-Stokes equation, which we have solved numerically to predict the induced ETP flow. The Navier-Stokes equation was solved by coupling the heat transfer module with the laminar flow module in COMSOL Multiphysics to determine the velocity distribution in the fluid.

4. Thermophoresis and Drag Force

Thermophoresis is a phenomenon that causes particles to migrate in the presence of a thermal gradient. Researchers have demonstrated in several ways to localize and control single nanoparticles by generating local temperature gradient field[32–34]. When a positive thermophoresis takes place, the particles will be pushed away from the hot region along the thermal gradient decreasing direction. It is imperative to note that the presence of the spatially dislocated hotspot in the external periphery of a hybrid dielectric-metal nanostructure can achieve (1) preventing the particles moving towards the hot region and (2) drive the particles to the optical trapping area. Here in this section, we explain the thermophoretic force on the particles. The thermophoretic force is expressed as[35]

$$\mathbf{F}_{\mathrm{th}} = -K_{\mathrm{B}}S_{\mathrm{T}}T(\mathbf{r})\nabla \mathrm{T},$$

where the K_{B} is the Boltzmann constant, and S_{T} is the Soret coefficient that $S_{\mathrm{T}} = D_{\mathrm{T}}/D$. The D_{T} is the thermophoretic mobility where[36]

$$D_{\mathrm{T}} = -\frac{\varepsilon}{2\eta T}\frac{2\Lambda_l}{2\Lambda_l+\Lambda_p}\left(1+\frac{\partial \ln\varepsilon}{\partial \ln T}\right)\zeta^{2}.$$

In the equation, Λ_l and Λp are thermal conductivities of the solvent and the particle respectively. The permittivity of the solvent in the electric double layer depends on surface charge density (around the particle), temperature, and ionic strength, where in the water $\frac{\partial \ln \varepsilon}{\partial \ln T} = -1.4$ at room temperature[36]. The surface charge density is characterized by the zeta potential ζ. For experiments in water medium without ionic surfactants, the thermophoretic force is a positive thermophoretic force, which will repel particles away from the hot Au block[37], which implies they particles will be pushed towards the slot cavity of the Si disk. Thus, the proposed hybrid platform provides a means to leverage the positive thermophoretic force in a synergistic manner with the optical gradient force to aid in the trapping process.

The drag force from the ETP flow overcome the thermophoretic force at the external region of the Au block before the particle will be transported to the slot cavity of the Si disk. The drag force exerted on the particles can be obtained from Stoke's law, which is given by[38]

$$\mathbf{F}_{\text{drag}}(\mathbf{r}) = \gamma \mathbf{v}(\mathbf{r}).$$

Here, γ is the Stokes drag coefficient according to Faxen's correction which accounts for frictional effects near the solid surfaces and is by

$$\gamma = \frac{6\pi\eta R}{\left[1 - \frac{9}{16}\left(\frac{R}{h}\right) + \frac{1}{8}\left(\frac{R}{h}\right)^3 - \frac{45}{256}\left(\frac{R}{h}\right)^4 - \frac{1}{16}\left(\frac{R}{h}\right)^5\right]}$$

, where η is the viscosity of the water, R is the radius of the particles, h is the distance from the center of the particle to the solid surface, and $\boldsymbol{v}(\boldsymbol{r})$ is the fluid flow velocity. For the smaller size particles, the behavior is determined by both diameter of the spheres and the viscosity of the fluid. Hence according to the specific fluid flow condition here, the drag force will keep the small particles moving in vortices and it is expected to be delivered by the thermophoretic force and trapped by optical force when it comes close.

Chapter II. Related Works

There are many methods have been introduced in the nanoscale optical trapping and manipulation. To achieve the stably trapping, plasmons enhanced optical forces are developed for the common method to generate strong optical force on nanoparticles. Several designs has been introduced before, such as the nanoantennas[12,39], nanoholes[40] and bowtie structures[41,42]. The fundamental physics principle of those structure is basing on the surface plasmon polaritons(SPP), where the light intensity hotspot close to the surface of the plasmonic nanostructure could reach thousands of times than the source intensity[41]. Therefore, the gradient force dominates at this scenario and since the optical gradient force is proportional to the light intensity gradient, the particles can be tightly trapped towards the hotspot. Another way to efficiently control nanoscale particles is that using the plasmon induced thermal effect to achieve the stably trapping by generating the fluid flow condition. Wang et al.[7] has proposed to use a plasmonic nanotweezer, i.e. gold nanopillar, to achieve an integrated heat sink and complete the trapping and manipulation of particles. Justus et al.[43] has introduced the on chip electrothermoplasmonic device that convert the loss into long range and rapid particles transportation with using plasmonic nanoantennas. Hong et al.[29] proposed and demonstrated a opto-thermo-electrohydrodynamic tweezers that can trap the particles in a far distance away from the laser spot area, which eliminates the heating damage. In this case, we notice that it is very necessary to avoid the high temperature region while taking the merits of their long-range fluid flow condition to achieve particles transportation.

Considering addressing the problem of the unnecessary plasmonic heating effect, researchers paid their attention on the low loss materials to achieve nanoscale optical trapping while generating negligible heating comparing with the plasmonic nanostructure. Zhe et al.[44] proposed the optical trapping with using entire silicon nanoantenna system. They demonstrated that the temperature rise is small enough (0.04 K) to be ignored when the trapping occurs. This could be greatly helpful in applying to the trapping of biological objects and quantum dots[44]. However, as shown in the paper, the electric field enhancement is only 6 times the source light, which is comparably much smaller than the plasmonic platform, hence impairs the strength of the optical trapping force.

In this thesis, we proposed the anapole assisted dielectric -metal hybrid nanostructure which shows its ability to achieve 30 times electric field enhancement and comparably controllable low temperature rise, which is a powerful platform for the biology sample and quantum emitters trapping experiments. Furthermore, the plasmonic counterparts provide the plasmon induced thermal effect that inducing long-range particles transportation, which is very important in completing fast optical trapping process.

Chapter III. Materials and Methods

1. Multiphysics modeling

The Finite Difference Time Domain method was implemented to calculate the electromagnetic simulation of the designed optical cavity plarform. We used a commercially available software Lumerical to handle the simulation process. In our simulation, we set the incident light as a plane wave with its polarization direction along x direction from the top of the nanoantenna with using the total-field scattered-field (TFSF) source. The background index was set as water (n=1.33), the SiO_2 was set as n=1.46 and the Si and Au layer index were set as Palik and Johnson-Christy respectively. We set different meshes for different structure domains as the requirement of reducing the error and complying with the computer memory requirement. The boundary condition was set as perfect match layer (PML). The electric field enhancement was calculated around the silicon nanodisk, and the scattering cross section is defined as

$$\sigma_{sc} = \left(\frac{1}{I_0}\right) \iint (\mathbf{n} \cdot \mathbf{S_{sc}}) ds$$

Where I_0 is the source intensity and $\mathbf{S_{sc}}$ is the Poynting vector. The monitor was set outside the TFSF source to collect the scattering energy.

We also used COMSOL Multiphysics (v 5.5) simulation software to simulate the electromagnetic field, heat transfer and fluid flow conditions. The simulations of the electromagnetic field were governed by the time independent wave equation

$$\nabla \times \nabla \times \mathbf{E} - k_0^2 \varepsilon(\mathbf{r}) \mathbf{E} = 0.$$

In the equation, E is the electric field and k_0 is the free-space wavenumber and $\varepsilon(\mathbf{r})$ is the position dependent complex permittivity. In COMSOL Multiphysics simulation, the "Wave Optics Module" is applied to calculate the electromagnetic field distribution and the optical force. Two steps are used in the numerical calculation process, i.e. solving the background field first and then calculating the scattered field with nanostructure. PMLs boundaries are applied as the boundary condition of the physical domain. The optical constant of Au is taken from the data of Johnson and Christy[2]. Then we use heat transfer module to solve the temperature distribution. The heat dissipation density was calculated as following

$$Q = \frac{1}{2} \mathbf{Re}(\mathbf{J} \cdot \mathbf{E}^*),$$

where **E** is the electric field distribution obtained from the solution of the electromagnetic wave equation, and **J** is the induced current density. The initial temperature and outer boundaries temperature are set to be 293.15 K. By taking the absorbed heat power dissipation density in the silicon nanoantenna from the optics simulation, we apply it as the heat source power of the subsequent heat transfer calculation. The thermal parameter of all the material are taken from COMSOL material library. In the simulation of the heat transfer module, we define the heat source density in the Au film with using following equation by considering the gaussian distribution of the laser beam

$$q(\mathbf{r}) = P_0(1 - R_C) \frac{\alpha_C}{\pi \sigma^2} e^{-\left(\frac{r^2}{2\sigma^2}\right)} e^{-\alpha_C z}$$

, where P_0 is the laser power, R_C is the reflectance of the Au film of 150 nm thickness, and α_C is the attenuation coefficient of the Au film which is defined as $\alpha_C = \frac{4\pi k}{\lambda}$, and k is the imaginary part of the complex refractive index of the Au layer[3,4].

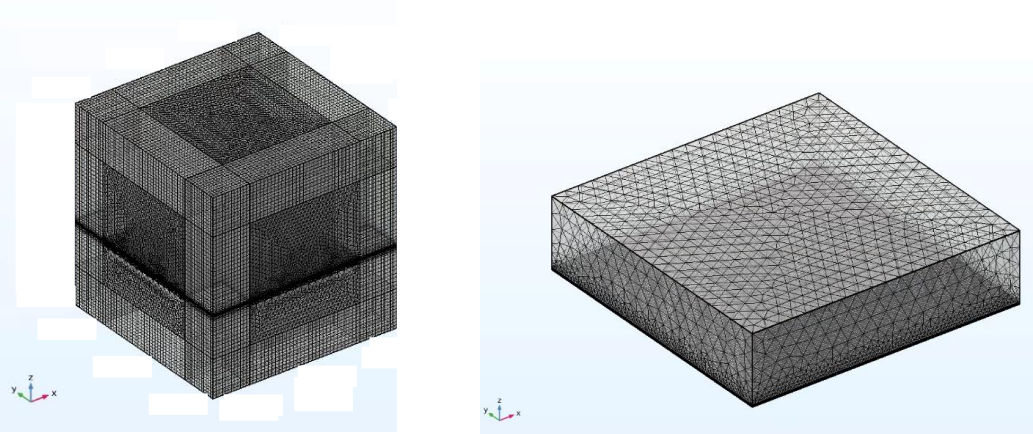

Figure 1 Simulation domain geometry. The hybrid nanoantenna is placed at the center of the domain on top of the Au film and SiO_2. Here in the figure the meshed domain for the EM simulation has been shown in a smaller domain, while the heat transfer and microfluid simulation will be processed in a larger domain.

Here we discuss the using of a commercial solver (COMSOL Multiphysics) for the simulations. The optical simulation domain has been shown in the Figure 1 with meshes applied. In the first program, the optics module has been applied on the silicon nanodisk and associated nanoantenna system. The proposed system comprises of an individual nanoantenna including a Si nanodisk with a narrow slot that is placed on a dielectric spacer and an Au reflector layer. The radius of the Si nanodisk is set as R=560 nm, while the height is set as H=100 nm. There is a narrow slot on the surface of the Si nanodisk antenna to make the electromagnetic field accessible to the suspended objects that will be trapped. In our optimized design, we have selected a slot with a depth of 40 nm, a width of 20 nm, and a length of 300 nm. The thickness of the Au film reflector layer that is placed under the Si nanoantenna to reflect the incident light and control the reflection phase of the light matching within the Si nanoantenna is set as 150 nm. The dielectric spacer between the nanoantenna and Au film is designed to have a thickness of 20 nm and the material is chosen as SiO_2 with a refractive index n=1.4565. Four Au blocks are placed around the Si nanodisk with a 150 nm distance away from the nanodisk for heat generation without perturbing the anapole mode inside the dielectric nanoantenna. The Au blocks have smaller sizes in comparison with the dielectric nanodisk. The environment surrounding the Si disk is set as water (n=1.33) which is widely used for optical trapping experiments. The whole structure is illuminated with a plane wave at normal incidence with its intensity setting as 1.11 mW/μm^2, which determine the optical trapping force and the following heating effect. The full scattering field calculation domain is a 5 × 5 × 5 μm cube, which includes the physical domain and the perfectly matched layer (PML) of 1 μm thickness.

The second program we used here includes the model of the heat transfer module, electrostatics module and laminar flow module, which are describing the environment that induced by ETP effect. As shown in the Figure 1, the domain is much larger than the optical simulation domain with a 100 × 100 × 10 μm^3 domain with a no-slip

wall condition. The initial and the boundary temperature is set as $T_0 = 293.15$ K. All the parameters of the materials thermal and electrostatics properties are applied from the COMSOL library database.

Chapter IV. Results

The proposed dielectric nanoantenna is depicted in the schematic Figure 2. This hybrid design comprises of an individual nanoantenna including a Si nanodisk with a narrow slot that is placed on a dielectric spacer and an Au reflector layer. The Au reflector layer along with the spacer acts as a metamaterial mirror[26,45]. We have tuned the geometrical parameters of the nanoantenna to ensure that the resonance wavelength is within the biological transparency window (i.e. 800 nm to 1200 nm). Since most of the enhanced electromagnetic field is within the volume of the Si nanodisk, we have introduced a narrow slot on the surface of the Si nanodisk antenna to make the electromagnetic field accessible to the suspended objects that will be trapped. Furthermore, the slot leads to a further enhancement of the electric field intensity by taking advantage of the continuity of the normal component of the displacement field[23], *i.e.* $D_{1n} = D_{2n}$ (or $\varepsilon_1 E_{1n} = \varepsilon_2 E_{2n}$). In the optimized design, we have selected the slot to achieve optimal performance, while also ensuring that the design is within the constraints of current nanofabrication capabilities. The thickness of the Au film reflector layer that is placed under the Si nanoantenna to reflect the incident light and control the reflection phase of the light matching within the Si nanoantenna is set as 150 nm. The dielectric spacer between the nanoantenna and Au film is designed to have a thickness of 20 nm and the material is chosen as SiO_2 with a refractive index n=1.4565. Four Au blocks are placed around the Si nanodisk with a 150 nm distance away from the nanodisk for heat generation without perturbing the anapole mode inside the dielectric nanoantenna. The Au blocks have smaller sizes in comparison with the dielectric nanodisk.

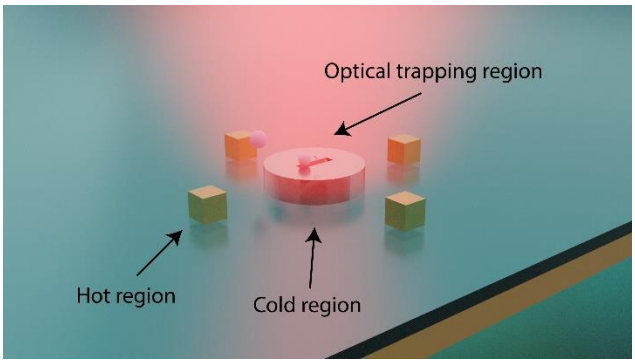

Figure 2. Schematic figure of dielectric-metal hybrid structure. A layer of Au film is positioned under the SiO2 spacer and on the top of the SiO2 substrate. Four Au blocks were placed around the Si nanodisk. Light is illuminated from the top of the structure, with its polarization direction perpendicular to the long axis of the slot. Particles are trapped in the slot cavity of the silicon disk which is a temperature minimum. The Au blocks provide thermal hotspots spatially dislocated from the electromagnetic hotspot in the slot cavity. The induced thermal hotspot is used for initiating electrothermoplasmonic flow for long-range transport of particles to the slot cavity.

1. Optical Performance

Figure 3(a) shows the electric field enhancement at various wavelengths. In the Si nanodisk, multiple orders of anapole modes can be generated at different resonance wavelengths, while the resonance wavelengths are a function of the nanodisk size[23]. Different anapole modes show different performance on light scattering property and the associated electric field enhancement. The introduction of the slot and the addition of the metallic (Au

film) reflector induces a slight shift in the resonance wavelength because this changes the effective dielectric volume and light path inside the structure. To compensate for the changes while designing the hybrid structure, the geometrical parameters of the Si nanodisk diameter is tuned to adjust the dielectric volume and the associated light path within the structure. In the optimized design, two electric field enhancement maxima are observed in the diagram, which denotes the anapole mode resonance positions corresponding to the dips in the scattering cross section spectrum[21]. The dips in scattering cross-section corresponding to field enhancement peaks from left to right are referred to as anapole mode 3 (AM3) and anapole mode 2 (AM2) as shown in Figure 3(a), and they give rise to high electric field enhancements inside the slot. Here, the anapole mode 2 (AM2) provides the best performance for confining light and generating high electric field enhancements inside the slot near the resonance wavelength of 1064 nm wavelength, which is within the biological transparency window and where the Si material and the surrounding water medium have low absorption.

As shown in Figure 3(b), the highest electric field intensity enhancement is mostly concentrated inside the slot where they are accessible to nanoscale objects suspended in the solution. In comparison to localized plasmonic resonance generated with a metallic nanoantenna, the mode volume of the anapole dielectric nanoantenna system is larger. A larger mode volume implies that the electromagnetic field is not tightly bound to deeply sub-wavelength volumes as typically obtained in the conventional plasmonic structure[18,46,47]. The limited confinement also implies an increased penetration of the evanescent field into the fluid medium. Given that optical gradient trapping force is proportional to the $|\nabla E|^2$ [30,48–50], this evanescent mode can readily interact with both small objects positioned inside the slot and larger size particles positioned near the top of the slot to achieve enhanced optical force.

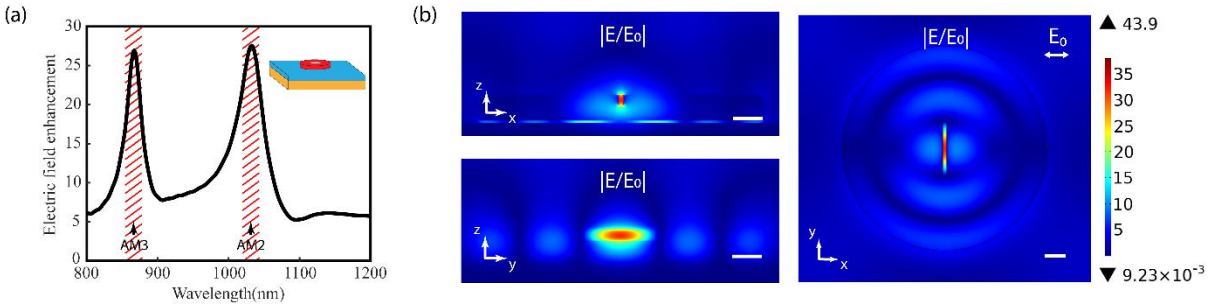

Figure 3 Electric field enhancement spectrum and distribution. (a) Electric field enhancement spectrum at the center of the slot in the Si nanodisk. Two anapole modes (AMs) have been denoted in the figure with the peak electric field enhancements. (b) Electric field enhancement distribution of the anapole mode nanodisk in XZ-plane (left upper panel), YZ-plane (left lower panel) and XY-plane (right panel) at the center of the nanoantenna. Scale bar represents 100 nm.

2. Plasmon Induced Thermal Effect

The heat dissipation in the Au reflector layer was accounted for by computing the total power absorbed in the Au film and adding this as a source term in the heat equation. The other heat source terms comprise of the electromagnetic power loss density in the Si disk and the Au blocks. We show the heat power dissipation density inside the dielectric nanoantenna for resonant illumination for both the designs of the Si nanodisk with Au blocks and the individual Si nanodisk. Through the heat dissipation density distribution, we could predict that most of

the heat dissipation occurs in the Au blocks, while the Si nanodisk contributes negligible heating effect to the system. The temperature distribution in the vicinity of the dielectric metal hybrid nanoantenna is depicted in Figure 4. The data shows that most of the temperature rise is in the Au blocks, while only a temperature rise of 1.5K is produced in the Si nanodisk. Thus, for this dielectric metal hybrid antenna system, the electromagnetic hotspot is at the slot cavity, which is a temperature minima, while the temperature maxima are displaced away from the position of the electromagnetic hotspot as depicted in Figure 4(c). this provides a platform that ensures that the optical trapped nanoscale objects do not experience pronounced heating effect at the trapping position with the high electromagnetic field intensity enhancement. This contrasts with plasmonic cavities where the electromagnetic hotspots are co-located with the thermal hotspots, which poses photothermal damage to delicate nanoscale objects. For the dielectric-metal hybrid system, the spatially-dislocated thermal hotspot may be used for initiating long-range electrothermal plasmonic flow for rapid transport of nanoscale particles to the low-loss dielectric slot for stable trapping, while overcoming the quenching or bleaching of quantum dots[51] and protecting biology samples from the irreversible photothermal damage of high temperature[52].

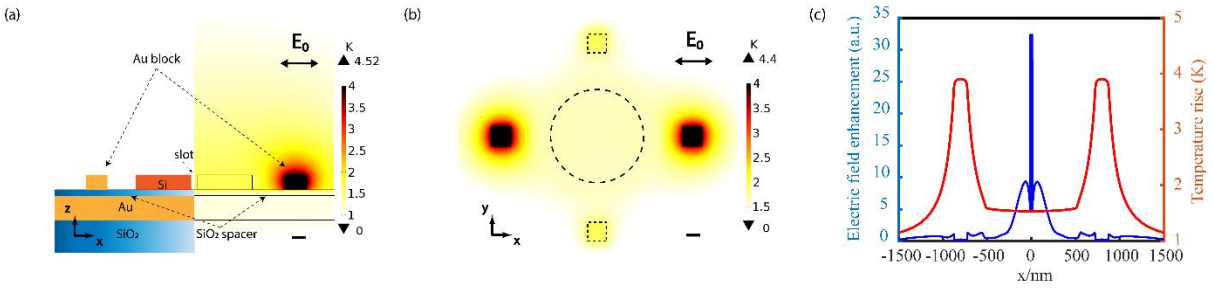

Figure 4 Temperature distribution around the dielectric-metal hybrid nanoantenna system. (a) Detail of the temperature distribution around the hybrid nanoantenna in the XZ-plane at the center of the hybrid structure. The temperature distribution is symmetric according to the center line. In this situation the illumination light polarization direction is along the short axis of the slot. (b) Temperature rise in XY-plane at the center of the hybrid nanoantenna. The higher temperature rise for the two Au blocks along the X-axis (polarization direction) arise because they experience higher heat dissipation density along this direction (c) Temperature rise and electric field enhancement distribution along the center of the slot as a function of position along the X direction at z_0=5 nm away from the top surface. The illumination light intensity is set as I_0=1.11 mW/μm2. The scale bar represents 100 nm for all the figure.

3. Optical Force and Trapping Potential

The trapping forces on the particles with size of 20 nm along the z direction in our hybrid nanoantenna system are depicted in Figure 5(a). In Figure 5(b), the trapping force along the z-axis on smaller particles with 10 nm and 15 nm diameter are shown, depicting the ability to trap particles with sizes smaller than the width of the cavity within the cavity. Figure 5(c), (d) show the optical force and associated trapping potential along the short axis of the slot. These particles with sizes set as 20 nm, 40 nm diameter PSs are positioned at a distance of 5 nm from the top surface of the Si nanodisk. Along the direction of long axis of the slot, the results in Figure 5 (e), (f) shows several trapping potential wells with varying depths for different sizes of PSs with diameters of 20 nm and 40 nm. However, the maximum trapping potential is at the center of the slot where the field enhancement is maximum, and this is the position where the particles with be preferentially trapped with the highest trapping stability. The

optical force here is approximately 4 times larger than the previous numerical calculation of dielectric nanoantenna on 20nm size PS particles in z direction, which shows a higher quality of trapping nanoscale objects.

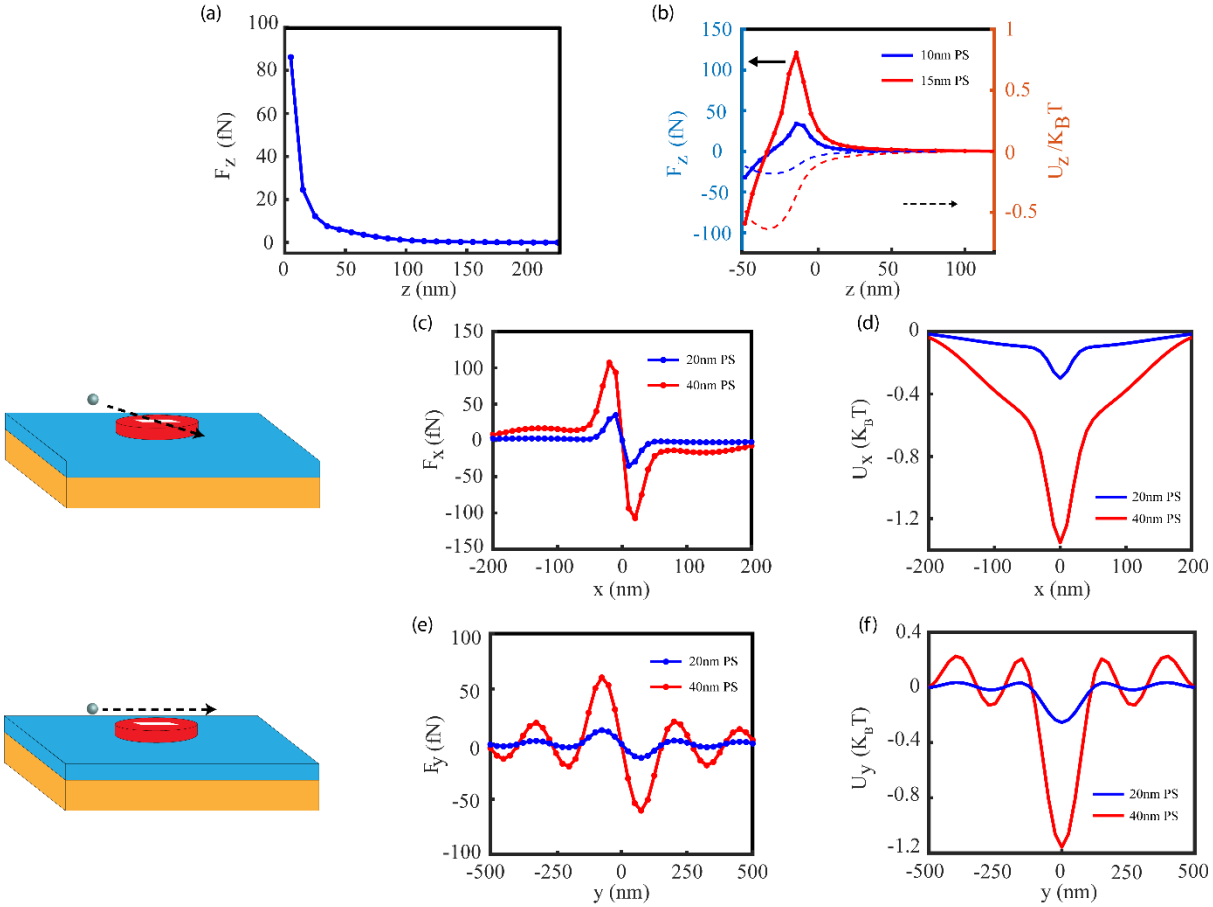

Figure 5 Optical trapping force and trapping potential. (a) Optical force along the Z-direction on 20nm polystyrene sphere (PS) on top of the anapole nanoantenna at xcenter=0 and ycenter=0 position. The position of z=0 denotes the top surface plane of the nanoantenna. The illumination light intensity is set as I0=1.11 mW/μm2. (b) Z-direction optical force (solid lines with dots) and trapping potential (dashed lines) on small PSs with 10 nm and 15 nm spheres trapped toward the slot at xcenter=0 and ycenter=0 position. The position of z=0 denotes the top surface plane of the nanoantenna. (c) Optical trapping force versus position along the x-direction for 20 nm and 40nm PSs. The particle sphere bottom is 5 nm away from the top surface of the anapole nanodisk. (d) Associated trapping potential along x-direction with the particle center at ycenter = 0 position. $1K_BT$=4.05×10-21J. (e) Optical trapping force versus position along the y-direction for 20 nm and 40 nm PSs. The particle sphere bottom is 5 nm away from the top surface of the anapole nanodisk. (f) Associated trapping potential along y-direction with the particle center at xcenter = 0 position. $1K_BT$=4.05×10-21J.

4. Long Range Particles Transportation

To demonstrate the long-range particles transportation, we use the laminar flow module in COMSOL Multiphysics for the fluid flow condition simulation. As shown in Figure 6, a vortex has been generated inside the fluid environment as a result of the nanoscale heating source derived from EM and heat transfer calculation. Above the center of the hybrid nanoantenna, there is a fluid flow maximum position shows on the top, which reaches 100 μm/s, within the thermal condition of 1.5K increase as shown in Figure 4. The particles are expected to be

transported first and then stably trapped at the center of the slot with the collaboration of fluid force and the optical trapping.

In Fiugre 6 (c), the thermophoretic force has been shown to demonstrate the assisting transportation from the high temperature region to the low temperature position, i.e. the center of the slot. The arrow and the color mapping show the force direction and magnitude explicitly, denoting the particles that close to the Au bars will experience larger positive thermophoretic force towards the center. In figure 6 (b), (d), the radial velocity of fluid flow and the total force exerted on 20nm diameter particles has been shown in the cut plane with 5 μm distance away from the top surface. The results show the particles will be transported towards the center.

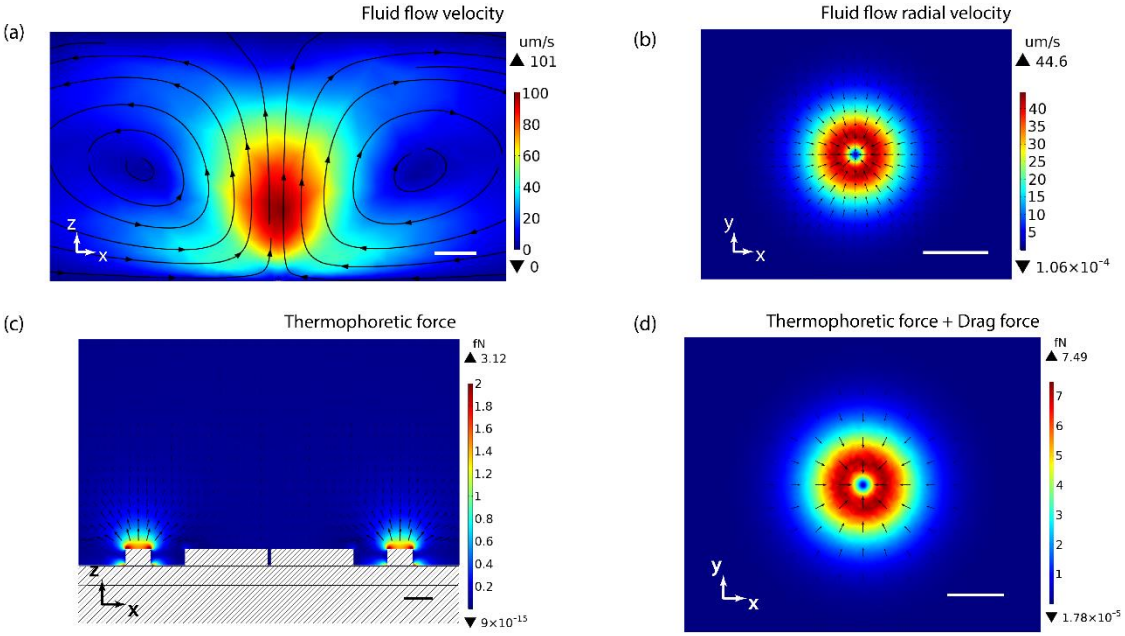

Figure 6 Fluid flow condition and the force exerted on the particles. (a) Fluid flow velocity profile at the center cut plane of the nanoantenna. The arrow shows the fluid flow direction, and the color mapping shows its velocity magnitude. (b) Radial fluid flow velocity profile on top of the nanoantenna in XY-plane. (c) Thermophoretic force in XZ-plane at the center. The vector represents the thermophoretic force direction, which is pointed away from the thermal hotspot (positive thermophoresis). The color mapping and saturated color map shows the force magnitude and distribution. (d) Total force (thermophoretic force and fluidic drag force) around the nanoantenna. The arrow shows that the force is consistently pointing inside towards the slot cavity. In the above simulations, the illumination intensity is the same as for previous simulations. The scale bar represents 10 um for (a)(b)(d) and 100 nm for (c).

Chapter V. Conclusion

We have presented numerical simulations demonstrating the optimal design of dielectric-metal hybrid nanoantenna by supporting anapole modes to achieve enhanced electromagnetic fields comparable to plasmonic systems, while separating the electromagnetic and thermal hotspot to generate both enhanced optical radiant force and long-range particle transport while ensure that the particles are trapped at the region of low temperature. Furthermore, we showed strong optical forces and tight trapping potentials for the stable trapping of nanoscale dielectric objects in our platform. Beyond the optical trapping, by inducing the fluid flow condition through the controllable limited thermal effect, a long-range transportation could also be harnessed on nano-size particles. Since the particles are trapped at the electromagnetic hotspots with minimal temperature rise, our proposed platform will provide the means to perform single particle enhanced spectroscopy of delicate biological samples with high trapping speeds, as well as a means to enhance the emission properties of nanoscale quantum emitters for quantum photonics applications.

REFERENCES

1. Ashkin, A. Atomic-Beam Deflection by Resonance-Radiation Pressure. *Phys. Rev. Lett.* **25**, 1321–1324 (1970).
2. Chu, S. Nobel Lecture: The manipulation of neutral particles. *Rev. Mod. Phys.* **70**, 685–706 (1998).
3. Cohen-Tannoudji, C. Manipulating atoms with photons. *Phys. Scr.* **1998**, 33 (1998).
4. Ashkin, A., Dziedzic, J. M., Bjorkholm, J. E. & Chu, S. Observation of a single-beam gradient force optical trap for dielectric particles. *Opt. Lett.* **11**, 288 (1986).
5. PELTON, M. *et al.* Optical trapping and alignment of single gold nanorods by using plasmon resonances. *Opt. Lett.* **31**, 2075–2077 (2006).
6. Hansen, P. M., Bhatia, V. K., Harrit, N. & Oddershede, L. Expanding the Optical Trapping Range of Gold Nanoparticles. *Nano Lett.* **5**, 1937–1942 (2005).
7. Wang, K., Schonbrun, E., Steinvurzel, P. & Crozier, K. B. Trapping and rotating nanoparticles using a plasmonic nano-tweezer with an integrated heat sink. *Nat. Commun.* **2**, 469 (2011).
8. Hong, C., Yang, S. & Ndukaife, J. C. Optofluidic control using plasmonic TiN bowtie nanoantenna [Invited]. *Opt. Mater. Express* **9**, 953–964 (2019).
9. Garcia-Guirado, J. *et al.* Overcoming Diffusion-Limited Biosensing by Electrothermoplasmonics. *ACS Photonics* **5**, 3673–3679 (2018).
10. Baffou, G. & Quidant, R. Thermo-plasmonics: Using metallic nanostructures as nano-sources of heat. *Laser and Photonics Reviews* vol. 7 171–187 (2013).
11. Alsawafta, M., Wahbeh, M. & Truong, V.-V. Simulated Optical Properties of Gold Nanocubes and Nanobars by Discrete Dipole Approximation. *J. Nanomater.* **2012**, 1–9 (2012).
12. Gordon, J. P. Radiation Forces and Momenta in Dielectric Media. *Phys. Rev. A, Gen. Phys.* **8**, 14–21 (1973).
13. Kravets, V. G., Kabashin, A. V., Barnes, W. L. & Grigorenko, A. N. Plasmonic Surface Lattice Resonances: A Review of Properties and Applications. *Chem. Rev.* **118**, 5912–5951 (2018).
14. Ndukaife, J. C. *et al.* Photothermal Heating Enabled by Plasmonic Nanostructures for Electrokinetic Manipulation and Sorting of Particles. *ACS Nano* **8**, 9035–9043 (2014).
15. Pang, Y. & Gordon, R. Optical trapping of a single protein. *Nano Lett.* **12**, 402–406 (2012).
16. Yesilkoy, F. *et al.* Ultrasensitive hyperspectral imaging and biodetection enabled by dielectric metasurfaces. *Nature Photonics* (2019) doi:10.1038/s41566-019-0394-6.
17. Gramotnev, D. K. & Bozhevolnyi, S. I. Nanofocusing of electromagnetic radiation. *Nat. Photonics* **8**, 13–22 (2014).
18. Schuller, J. A. *et al.* Plasmonics for extreme light concentration and manipulation. *Nat. Mater.* **9**, 193–204 (2010).
19. Ho, C. M. & Scherrer, R. J. Anapole dark matter. *Phys. Lett. B* **722**, 341–346 (2013).
20. Miroshnichenko, A. E. *et al.* Nonradiating anapole modes in dielectric nanoparticles. *Nat. Commun.* **6**, 8069 (2015).
21. Wei, L., Xi, Z., Bhattacharya, N. & Urbach, H. P. Excitation of the radiationless anapole mode. *Optica* **3**, 799–802 (2016).
22. Savinov, V., Papasimakis, N., Tsai, D. P. & Zheludev, N. I. Optical anapoles. *Commun. Phys.* **2**, 69 (2019).
23. Yang, Y., Zenin, V. A. & Bozhevolnyi, S. I. Anapole-Assisted Strong Field Enhancement in Individual All-Dielectric Nanostructures. *ACS Photonics* **5**, 1960–1966 (2018).
24. Yang, Y. *et al.* Multimode directionality in all-dielectric metasurfaces. *Phys. Rev. B* **95**, 165426 (2017).
25. Totero Gongora, J. S., Favraud, G. & Fratalocchi, A. Fundamental and high-order anapoles in all-dielectric metamaterials via Fano–Feshbach modes competition. *Nanotechnology* **28**, 104001 (2017).
26. Sabri, L., Huang, Q., Liu, J.-N. & Cunningham, B. T. Design of anapole mode electromagnetic field enhancement structures for

biosensing applications. *Opt. Express* **27**, 7196–7212 (2019).

27. Grinblat, G., Li, Y., Nielsen, M. P., Oulton, R. F. & Maier, S. A. Enhanced Third Harmonic Generation in Single Germanium Nanodisks Excited at the Anapole Mode. *Nano Lett.* **16**, 4635–4640 (2016).
28. Shibanuma, T., Grinblat, G., Albella, P. & Maier, S. A. Efficient Third Harmonic Generation from Metal–Dielectric Hybrid Nanoantennas. *Nano Lett.* **17**, 2647–2651 (2017).
29. Hong, C., Yang, S. & Ndukaife, J. C. Stand-off trapping and manipulation of sub-10 nm objects and biomolecules using opto-thermo-electrohydrodynamic tweezers. *Nat. Nanotechnol.* (2020) doi:10.1038/s41565-020-0760-z.
30. Ndukaife, J. C. *et al*. Long-range and rapid transport of individual nano-objects by a hybrid electrothermoplasmonic nanotweezer. *Nat. Nanotechnol.* **11**, 53–59 (2016).
31. Ramos, A., Morgan, H., Green, N. G. & Castellanos, A. Ac electrokinetics: a review of forces in microelectrode structures. *J. Phys. D. Appl. Phys.* **31**, 2338–2353 (1998).
32. Lin, L. *et al.* Thermophoretic Tweezers for Low-Power and Versatile Manipulation of Biological Cells. *ACS Nano* **11**, 3147–3154 (2017).
33. Iacopini, S. & Piazza, R. Thermophoresis in protein solutions. *Europhys. Lett.* **63**, 247–253 (2003).
34. Lin, L. *et al.* Opto-thermoelectric nanotweezers. *Nat. Photonics* **12**, 195–201 (2018).
35. Burelbach, J., Zupkauskas, M., Lamboll, R., Lan, Y. & Eiser, E. Colloidal motion under the action of a thermophoretic force. *J. Chem. Phys.* **147**, 94906 (2017).
36. Derjaguin, B. V, Churaev, N. V & Muller, V. M. Surface Forces in Transport Phenomena BT - Surface Forces. in (eds. Derjaguin, B. V, Churaev, N. V & Muller, V. M.) 369–431 (Springer US, 1987). doi:10.1007/978-1-4757-6639-4_11.
37. Lin, L. *et al.* Opto-thermoelectric nanotweezers. *Nat. Photonics* **12**, 195–201 (2018).
38. Yang, G., Zhang, H., Luo, J. & Wang, T. Drag force of bubble swarms and numerical simulations of a bubble column with a CFD-PBM coupled model. *Chem. Eng. Sci.* **192**, 714–724 (2018).
39. Righini, M. *et al.* Nano-optical Trapping of Rayleigh Particles and Escherichia coli Bacteria with Resonant Optical Antennas. *Nano Lett.* **9**, 3387–3391 (2009).
40. Pang, Y. & Gordon, R. Optical Trapping of 12 nm Dielectric Spheres Using Double-Nanoholes in a Gold Film. *Nano Lett.* **11**, 3763–3767 (2011).
41. Hong, C., Yang, S. & Ndukaife, J. C. Optofluidic control using plasmonic TiN bowtie nanoantenna. *Opt. Mater. Express* **9**, 953 (2019).
42. Roxworthy, B. J. *et al.* Application of Plasmonic Bowtie Nanoantenna Arrays for Optical Trapping, Stacking, and Sorting. *Nano Lett.* **12**, 796–801 (2012).
43. Ndukaife, J. C. *et al*. Long-range and rapid transport of individual nano-objects by a hybrid electrothermoplasmonic nanotweezer. *Nat. Nanotechnol.* **11**, 53–59 (2016).
44. Xu, Z. & Crozier, K. B. All-dielectric nanotweezers for trapping and observation of a single quantum dot. *Opt. Express* **27**, 4034 (2019).
45. Esfandyarpour, M., Garnett, E. C., Cui, Y., McGehee, M. D. & Brongersma, M. L. Metamaterial mirrors in optoelectronic devices. *Nat. Nanotechnol.* **9**, 542–547 (2014).
46. Xu, Z., Song, W. & Crozier, K. B. Direct Particle Tracking Observation and Brownian Dynamics Simulations of a Single Nanoparticle Optically Trapped by a Plasmonic Nanoaperture. *ACS Photonics* **5**, 2850–2859 (2018).
47. Santhosh, K., Bitton, O., Chuntonov, L. & Haran, G. Vacuum Rabi splitting in a plasmonic cavity at the single quantum emitter limit. *Nat. Commun.* **7**, ncomms11823 (2016).
48. Ashkin, A. Optical trapping and manipulation of neutral particles using lasers Notes : Optical trapping and manipulation of neutral particles. (2006) doi:10.1073/pnas.94.10.4853.

49. Ashkin, A. & Dziedzic, J. Optical trapping and manipulation of viruses and bacteria. *Science (80-.).* **235**, 1517–1520 (1987).

50. Kowal, J. *et al.* Proteomic comparison defines novel markers to characterize heterogeneous populations of extracellular vesicle subtypes. *Proc. Natl. Acad. Sci. U. S. A.* **113**, E968–E977 (2016).

51. Regmi, R. *et al.* All-Dielectric Silicon Nanogap Antennas To Enhance the Fluorescence of Single Molecules. *Nano Lett.* **16**, 5143–5151 (2016).

52. Donner, J. S., Baffou, G., McCloskey, D. & Quidant, R. Plasmon-Assisted Optofluidics. *ACS Nano* **5**, 5457–5462 (2011).